Investigation of the Impact of Reduced Density Low-GWP Refrigerants in a Commercial R-410A Scroll Compressor

Graham Alexander Tyra[1]*, Shahzad Yousaf[2,] Craig R. Bradshaw[3]

[1,2,3]Oklahoma State University, Department of Mechanical and Aerospace Engineering, Stillwater, Ok, United States
[1]gtyra@okstate.edu
[2]shahzad.yousaf@okstate.edu
[3]craig.bradshaw@okstate.edu

ABSTRACT

With the recent legislation passed to reduce the effect emissions have on global temperatures causing the phase out of current third generation refrigerants, the industry has focused on creating equipment based on the fourth generation with a focus on low global warming potential. Research is needed to understand how components react when these new low GWP refrigerants are used, particularly in compressors. This work quantifies the impact in compressors with an experimental analysis of R-1234yf and R-444A in a 40-ton commercial scroll compressor that was designed for R-410A, using test data collected from a hot-gas bypass compressor load stand. Tests were performed for saturated suction temperatures ranging from 20 °F (-6.67 °C) to 60 °F (15.56 °C), saturated discharge temperatures from 80 °F (26.67 °C) to 120 °F (48.49 °C), shaft speeds from 45 Hz to 60 Hz, and superheats from 10 °F (5.56 °C) to 30 °F (16.67 °C) for a total of 22 data points for each compressor. Results show that R-410A performs significantly better in the scroll compressor than both R-1234yf and R-444A, while R-444A had a better compressor efficiency than R-1234yf, but a decrease in overall system performance. At peak performance, R-410A had an isentropic efficiency of 74.7% and a COP of 4.22, R-1234yf had an efficiency of 64.5% and a COP of 3.8, while R-444A had an efficiency of 66.6% and the lowest COP of 2.4.

1. INTRODUCTION

While the effort to limit the damage to the ozone layer by replacing older refrigerants with hydrofluorocarbons (HFCs) such as R-410A and R-134a has been successful, HFCs unfortunately have been a significant contributor to global warming. To mitigate this damage, the worldwide community has passed several new laws and regulations to begin the phaseout of refrigerants with a global warming potential (GWP) greater than 150. Unfortunately, no refrigerant exists that can satisfy both environmental and thermodynamic demands. A study done by Domanski and McLinden found by using a Pareto front created from thermodynamic properties such as the critical temperature and pressure, the acentric factor, and the ideal-gas heat capacity that there are limits to the performance even a theoretical refrigerant can have, and there is an inverse relationship between the COP and volumetric cooling capacity (McLinden et al., 2012). Further expanding on this, Domanski found a strong correlation between the critical temperature and the tradeoff between COP and volumetric cooling capacity (Domanski et al., 2014). After examining 56,000 molecules, McLinden only found 62 possible combinations that form refrigerants with an acceptable GWP and a critical temperature in a range to be effective in current refrigeration equipment (McLinden et al., 2014). Despite the losses in thermodynamic performance, it is necessary to maintain and improve upon current standards of system efficiency, making the improvement of refrigeration cycle components a top priority.

The scroll compressor was first proposed in 1905 as a rotary engine using two parallel plates with spiral bands wrapped around each other in what would become known as the fixed and orbiting scroll. As the scroll plates rotate around each other, the fluid would be displaced and compressed (Creux, 1905). Due to manufacturing constraints however, the scroll compressor was largely abandoned until the late 1970's and 1980's when the advantages of low noise, vibration, torque pulse, and gas pulsations were discovered (Elson, 2008). One of the most studied aspects in scroll compressor efficiency is the relationship between leakage and friction of the axial and radial clearance between the

two scroll plates, though the complex scroll geometry makes precise calculations difficult. Through CFD modeling, Sun calculated that the leakage through the axial clearance is greater than the tangential leakage (Sun et al., 2022). Cho found that higher pressure ratios reduced the tangential leakage, and that an increase in the radial clearance had a linear increase on the tangential leakage (Cho et al., 2000). Tip seals are commonly used to reduce axial leakage. Fukata analyzed how increasing the contact force on the tip seal resulted in a reduction in axial leakage but increased the frictional force of the compressor (Fukuta et al., 2020). Youn found that for various constant tip clearances, the tip leakage area decreases with increasing orbiting angle, and the leakage decreased with increasing pressure ratio (Youn et al., 2000). Additionally, as the downstream pressure approached the upstream pressure, Lee observed an increase in the tip clearance due to the decrease in tip sealing force (Lee et al., 2002). Tanveer and Bradshaw determined that the leakage area is the largest factor in the performance of the scroll compressor, and that using low pressure refrigerants would result in higher leakage areas (Tanveer and Bradshaw, 2021). The literature agrees that changing the suction and discharge pressures in the scroll compressor will change the leakage area and in turn the performance of the compressor. Changing the refrigerant used will naturally change this pressure ratio, though the power consumption, mass flow rate, and the thermodynamic properties of the refrigerant will change as well, further affecting the compressor and overall system performance. This study determines what performance losses are experienced in the compressor as well as the overall system by experimentally testing a commercial scroll compressor, designed for R-410A, with lower pressure, low-GWP, refrigerants R-1234yf and R-444A over a wide range of operating conditions.

2. METHODOLOGY

2.1 Refrigerant Selection

To exacerbate the influence of the working fluid, this study selected refrigerants (R-1234yf, and R-444A) with significantly different thermodynamic properties than the refrigerant the compressor was designed for (R-410A). The critical temperature is inversely related to the volumetric cooling capacity, and a lower vapor density will result in an increase in pressure drop and reduced capacity (Prapainop and Suen, 2012). Both R-1234yf and R-444A have higher critical temperatures and lower pressures than R-410A. R-410A has the lowest critical temperature, and highest vapor pressure and densities, though its GWP is on the order of magnitudes higher than both R-1234yf and R-444A. R-444A has a higher GWP and critical temperature than R-1234yf, but it has similar operating pressures and densities. While R-410A has an ASHRAE safety classification of A1; meaning non-toxic and non-flammable; both R-1234yf and R-444A are slightly flammable, giving them a classification of A2L. Table 1 shows the properties of these refrigerants.

Table 1: Selected Refrigerant Properties

Refrigerant	GWP	Critical Temperature in °F (°C)	Saturated Pressure @ 40 °F (4.44 °C) in psi (kPa)	Saturated Density @ 40 °F (4.44 °C) in lbm/ft^3 (kg/m^3)	Mass Basis Composition [%]	ASHRAE Safety Classification
R-410A	1890	160.42 (71.34)	133.05 (779.45)	2.20 (35.24)	R32/125 (50/50)	A1
R-1234yf	<1	202.46 (94.7)	53.12 (366.25)	1.272 (20.38)	Pure Fluid	A2L
R-444A	93	223.45 (106.36)	46.87 (323.16)	0.927 (15.01)	R32/152a/1234ze(E) (12/5/83)	A2L

2.2 Load Stand and Instrumentation

All testing was performed on a light-commercial compressor load stand with a maximum capacity of 80-tons. As detailed in (Schmidt et al., 2019), the load stand was designed as a hot-gas bypass featuring a main loop, a bypass loop, and an economizer loop which was not utilized in testing. Beginning at the compressor suction inlet, superheated refrigerant at a specific evaporating pressure will enter the compressor, where it will then exit with a higher discharge temperature and a selected condensing pressure. The refrigerant will then pass through a coalescent oil separator. After separation, the oil will be sent back into the compressor in a regulated flow, while the refrigerant will pass through a Coriolis mass flow meter. Once the rate of mass flow has been measured, the majority of the refrigerant will remain as a vapor and will bypass the condensers, while the rest of the refrigerant will enter the liquid line. The vapor refrigerant that bypasses the condensers will then reach three parallel expansion valves, where it will be expanded to

a selected evaporating pressure before being mixed back together with the refrigerant passing through the condensers. The refrigerant entering the liquid line will be condensed through two brazed plate heat exchangers connected to a chilled water supply, and then as a liquid pass through a receiver and a filter dryer before reaching another set of three parallel expansion valves to regulate the flow of liquid as it is mixed back together with the hot gas refrigerant to reach the desired suction conditions. Adjusting the vapor and liquid expansion valves allows for control of the suction pressure and temperature, while adjusting the flow of chilled water in the condensers will affect the discharge pressure. Finally, the refrigerant will pass through a secondary Coriolis mass flow meter before entering the compressor suction port again. A complete piping and instrumentation diagram (P&ID) of the hot-gas bypass load stand is shown in Figure 1. The compressor used in testing was a variable speed 40-ton Bitzer scroll compressor, model number GSD80485VAB4-1.

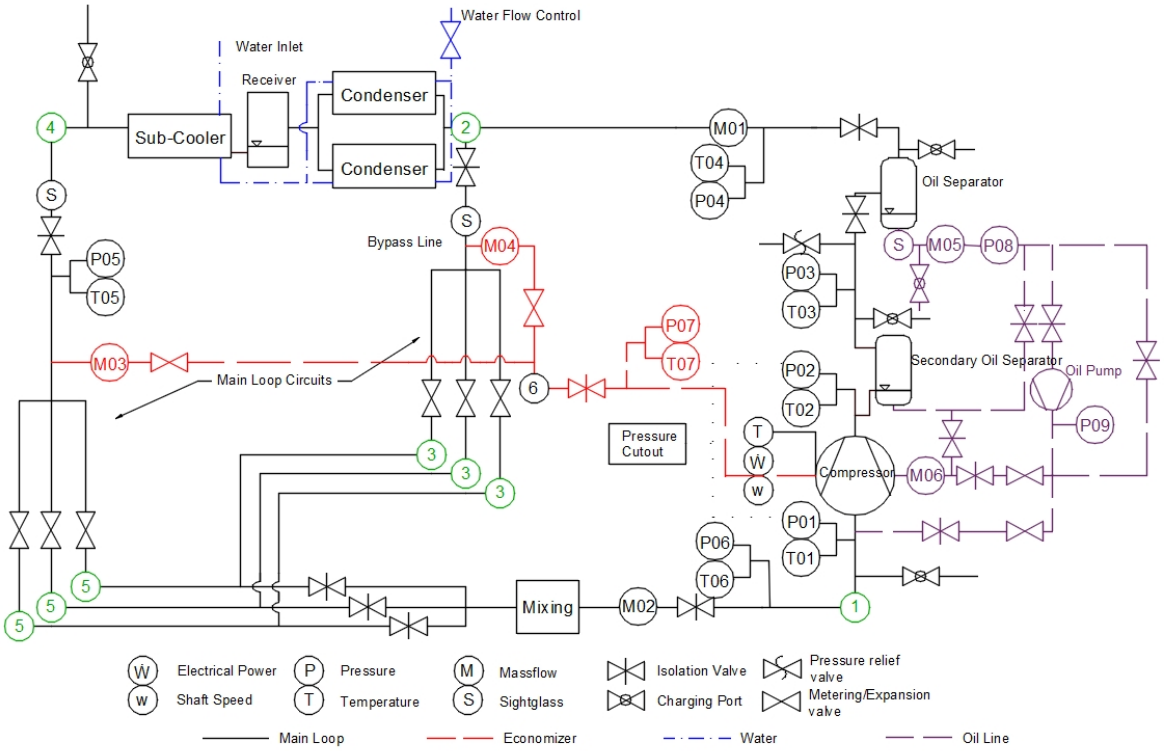

Figure 1: P&ID of hot-gas bypass load stand, modified from Schmidt et al. (2019).

Compressor performance is calculated through the generated mass flow rate and power consumption at given suction and discharge conditions. High accuracy pressure transducers and platinum RTD's were used to lower the potential for error in the measurements. As required in ASHRAE 23.1, two Coriolis mass flow meters were used as a redundancy; one measuring the suction mass flow rate, and another measuring the discharge mass flow rate which was used in the performance calculations. Power was supplied to the compressor through a 112 kW variable frequency drive (VFD), where the power was independently measured using a Watt transducer. Compressor speed is controlled through the VFD and measured through an accelerometer (Schmidt et al., 2019).

2.3 Testing Procedures

Both R-1234yf and R-444A were selected based on their GWP, operating pressures, and their potential for use as refrigerants of the future. To properly gauge their performance in the compressor, a wide test matrix consisting of a saturated suction temperature (SST) sweep, a saturated discharge temperature (SDT) sweep, a superheat sweep, as well as a speed sweep were selected for a total of twenty-two datapoints for each refrigerant. The SST sweep consists of five points ranging from 20 °F (-6.67 °C) to 60 °F (15.56 °C), with an increase of 10 °F (5.56°C) in the SST for each point. The superheat, speed, and SDT remained constant at 10 °F (5.56 °C), 60 Hz, and 100 °F (37.78 °C) respectively. The SDT sweep consisted of another five points ranging from 80 °F (26.67 °C) to 120 °F (48.89 °C), with the superheat and speed remaining constant at the same 10 °F and 60 Hz, while the SST remained constant at 40

°F (4.44 °C). In both the superheat and speed sweeps, the SST and SDT both remained constant at 40 °F (4.44 °C) and 120 °F (48.89 °C) respectively. The superheat sweep also consisted of five points, with the superheat increasing 5 °F (2.78 °C) for each point in a range from 10 °F (5.56 °C) to 30 °F (16.67 °C) while the speed remained constant at 60 Hz. Finally, the speed sweep increased from 45 Hz to 60 Hz, with a constant superheat of 10 °F (5.56 °C). Over all twenty-two datapoints, this test matrix provides an in-depth look at varying suction and discharge conditions of the refrigerant moving through the compressor, as well as a mechanical aspect of the compressor with the inclusion of the speed sweep. R-410A was simulated using Bitzer Software for the same points in the test matrix, apart from the speed sweep which was only able to be simulated at 50 Hz and 60 Hz. A complete test matrix is shown in Table 2.

Table 2: Test Matrix Points

	SST in °F (°C)	SDT in °F (°C)	Superheat in °F (°C)	Speed (Hz)
1	20 (-6.67)	100 (37.78)	10 (5.56)	60
2	30 (-1.11)			
3	40 (4.44)			
4	50 (10)			
5	60 (15.56)			
6	40 (4.44)	80 (26.67)	10 (5.56)	60
7		90 (32.22)		
8		100 (37.78)		
9		110 (43.33)		
10		120 (48.89)		
11	40 (4.44)	100 (37.78)	10 (5.56)	60
12				58
13				55
14				52
15				50
16				47
17				45
18	40 (4.44)	100 (37.78)	10 (5.56)	60
19			15 (8.33)	
20			20 (11.11)	
21			25 (13.89)	
22			30 (16.67)	

2.4 Performance Calculations

When the suction temperature, suction pressure, and discharge pressure reach steady state, the discharge temperature, mass flow rate, and power can be recorded, and using those values the conditions at each state are able to be calculated. Figure 3 shows the P-h diagram of the simulated cycle. Beginning at the compressor suction (state 1) enthalpy, entropy, and density are calculated as a function of suction pressure and temperature, and a function of discharge pressure and temperature at the compressor discharge (state 2). Since there is no evaporator in the hot-gas bypass style load stand, one must be simulated based on a basic vapor compression cycle. Assuming a fixed subcooling of 10 °F (5.56 °C), once the refrigerant exits the condenser (state 3), the temperature can be calculated as,

$$T_3 = T_{cond} - \Delta T_{subcool} \tag{1}$$

while the enthalpy can be calculated as a function of T_3 and the condensing pressure. Assuming isentropic expansion through the expansion valves (state 4).

$$h_4 = h_3 \tag{2}$$

To calculate the compressor performance metrics, the isentropic enthalpy of state 2 is found to be a function of discharge pressure and suction entropy. With this, the isentropic efficiency, can be calculated as,

$$\eta_{is} = \frac{\dot{m}(h_{2s} - h_1)}{\dot{W}} \quad (3)$$

Next the volumetric efficiency is calculated using the compressor volumetric displacement of $V_{disp} = 93.2\ m^3/h$ and the rotational speed (ω) in RPM with the formula,

$$\eta_{vol} = \frac{\dot{m}}{V_{disp} * \omega * \rho_1} \quad (4)$$

The cooling capacity and the COP are calculated as follows.

$$\dot{Q}_{cool} = \dot{m}(h_1 - h_4) \quad (5)$$

$$COP = \frac{\dot{Q}_{cool}}{\dot{W}} \quad (6)$$

2.5 Uncertainty Calculations

With any measurement there is a percentage of uncertainty in the result. All the instrumentation mentioned in Table 2 contributes to the propagated uncertainty of the performance calculations. The lower the accuracy a sensor has, the higher contribution that sensor will have to the propagated uncertainty of each result. Following the standard listed in ASME PTC 19.1 (2018), propagated uncertainty is calculated with equations 7 and 8.

$$\Theta_i' = \frac{\overline{X}_\iota}{R}\left(\frac{\delta R}{\delta \overline{X}_\iota}\right) \quad (7)$$

$$b_R \frac{b_R}{R} = \left[\sum_{i=1}^{I}\left(\Theta_i' \frac{b_{\overline{X}_\iota}}{\overline{X}_\iota}\right)^2\right]^{\frac{1}{2}} \quad (8)$$

The propagated uncertainty of the isentropic efficiency was found to be ± 1.8% and the COP had an uncertainty of ±0.13, with nearly 77% of the uncertainty in both results from the Watt transducer. The uncertainty of the volumetric efficiency was ±1.3%, with the mass flow meter as the largest contributor. Since R-410A was simulated, an uncertainty of ± 2.5% was applied to both the isentropic and volumetric efficiencies.

3. RESULTS

3.1 Behavior of mass flow rate, power and discharge temperature

All three refrigerants followed the same trends across all varied parameters in the test matrix, with a few exceptions. R-410A consistently had the best performance in every metric, followed by R-1234yf and R-444A. The discharge temperature did not show any notable trends across the speed, and superheat sweeps, with R-444A having an approximate 10% higher discharge temperature than R-1234yf and approximately 13% higher than R-410A. Lower SST and higher SDT conditions eventually led to the discharge temperature of R-410A to rise above R-1234yf at a SST = 30 °F (-1.11 °C) and a SDT = 110 °F (43.33 °C). Figure 2 shows this behavior in the SDT sweep.

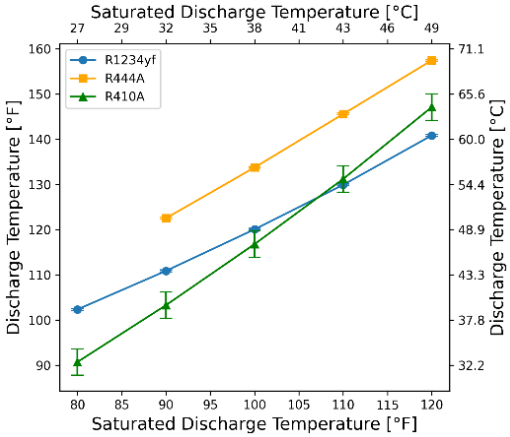

Figure 2: Discharge temperature vs SDT.

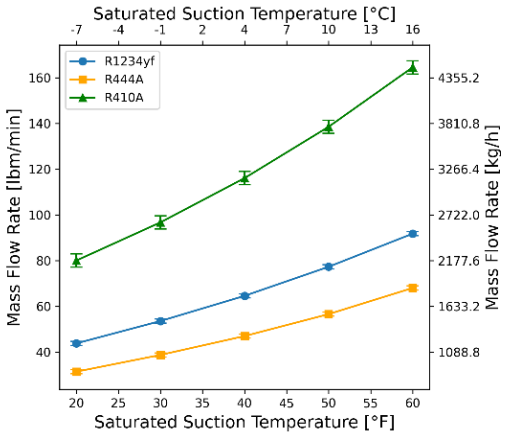

Figure 3: Mass flow rate vs SST.

A significant decrease in the mass flow rate from R-410A is observed when the low GWP refrigerants are used. At their peak mass flow rates, R-1234yf had a 44% reduction from R-410A. Additionally, R-444A had a much larger reduction of nearly 59% from R-410A at its peak, and nearly a 26% reduction from the mass flow rate of R-1234yf at its peak as well. The peak mass flow rate for all three refrigerants occurred at a SST = 60 °F (15.56 °C). More so, an increase in the SST led to the largest increase in mass flow rate as illustrated in Figure 3, and there was no meaningful change during the superheat sweep. As the speed decreased, so did the mass flow rate, while increasing the SDT also led to a slight decrease in mass flow rate.

R-410A had the largest power consumption of all three refrigerants, followed by R-1234yf and then R-444A. In fact, R-410A consumed roughly 55% more power than R-1234yf and 58% more power than R-444A. Despite R-444A having a 26% reduction in the mass flow rate from R-1234yf at its peak at a SST = 60 °F (15.56 °C), R-444A only used 6% less power than R-1234yf. Similar behavior is observed in every sweep, even though there was no notable change in the power consumption across the superheat sweep, and only a small increase in the power consumption with increasing SST. The largest increase in the power consumption of the refrigerants occurred with an increase in the compressor speed and SDT, shown in Figure 4.

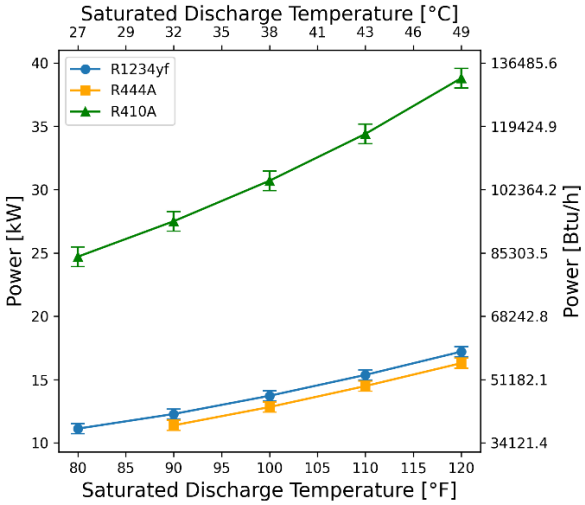

Figure 4: Compressor power consumption vs SDT.

3.2 Behavior of efficiencies, capacity, and COP

Isentropic efficiency is one of the most important metrics for judging compressor performance. As would be expected, R-410A had the highest isentropic efficiencies across every point in the test matrix, while having a general increase

of 10 to 15 percentage points when compared to R-444A and R-1234yf. Surprisingly, R-444A consistently had an isentropic efficiency 1-3 percentage points higher than R-1234yf across all points in the test matrix, despite having a lower mass flow rate. This can be attributed to the isentropic enthalpy difference that occurs between the compressor suction and discharge. When comparing the peak isentropic efficiency in the SST sweep at a SST = 40 °F (4.44 °C), R-444A had a 27.2% decrease in the mass flow rate from R-1234yf, but had a 32.9% higher isentropic enthalpy difference. At that same point, R-444A also consumed 6.4% less power than R-1234yf, which lead to R-444A having an isentropic efficiency that is 2 percentage points higher than R-1234yf. Every point in the test matrix also followed the trends exhibited between those two refrigerants. While R-410A had higher isentropic efficiencies than both R-1234yf and R-444A, the peaks occurred at different points between all three refrigerants. R-410A and R-1234yf both peaked at a SDT = 110 °F (43.33 °C) with an efficiency of 74.7% and 64.5% respectively, while R-444A peaked with an isentropic efficiency of 66.6% at a SDT = 120 °F (48.89 °C). In the SST sweep, R-410A peaked again at an isentropic efficiency of 74.7% at a SST = 30 °F. R-1234yf and R-444A peaked at a SST = 40 °F with an efficiency of 63.3% and 65.4% respectively. The isentropic efficiencies of both the SDT and SST sweeps can be found in Figure 5 and Figure 6 respectively.

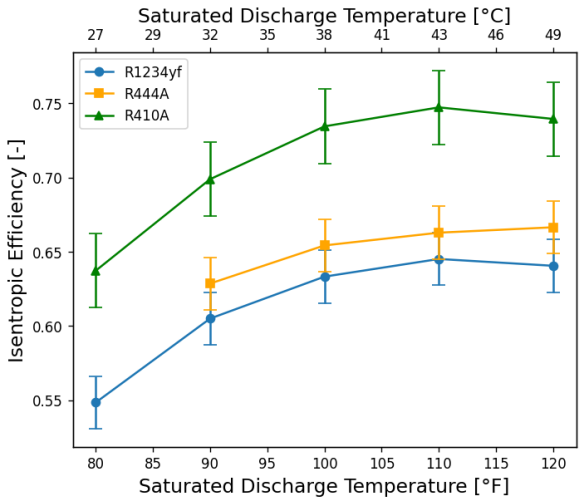

Figure 5: Isentropic efficiency vs SDT.

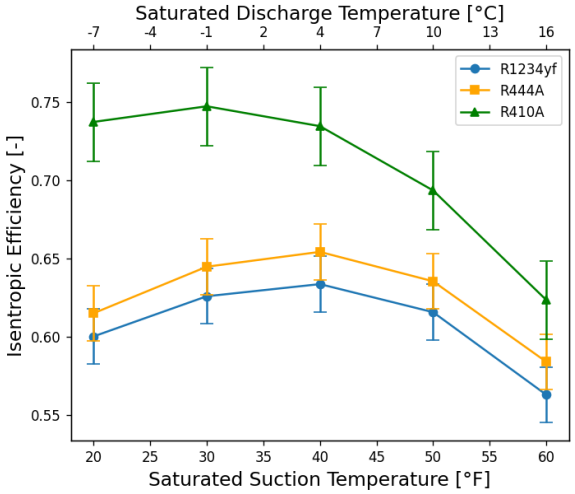

Figure 6: Isentropic efficiency vs SST.

Despite very different mass flow rates, both R-1234yf and R-444A had nearly identical volumetric efficiencies approximately 88% through the entire test matrix, though generally R-410A performed around 10 percentage points better than both low GWP refrigerants. There was no notable change in the volumetric efficiency in the superheat sweep, and a slight decrease in both the speed and SDT sweeps as the speed and SDT increased. Figure 7 illustrates the change in volumetric efficiency with increasing SST. All three refrigerants show an increase of approximately 3 percentage points, and while the volumetric efficiency of R-410A rises above 100% at an SST = 50 °F (10 °C), it is still within an acceptable range of error. The authors acknowledge that it is impossible to have volumetric efficiencies greater than 100%, as experienced by a small number of points in the R-410A data. Despite this impossibility, the authors chose to include this information because all data points are within possibility when the potential error is considered.

The cooling capacity follows the same trends as the mass flow rate. The peak capacity for all three refrigerants occurred at SST = 60 °F (15.56 °C), the same point as the peak mass flow rate. R-444A has a 44.1% decrease in capacity from R-1234yf, and a 71% decrease from R-410A. R-1234yf only had a 58% decrease in capacity when compared to R-410A. Figure 8 illustrates this behavior as well. The superheat had no major effect on the capacity, an increase in speed led to an increase in capacity, and an increase in SDT led to a decrease in capacity. Interestingly, despite R-444A having a greater isentropic enthalpy difference than R-1234yf, the opposite is true for the enthalpy difference in the evaporator. R-1234yf had about a 7% increase in the evaporator enthalpy difference from R-444A in every sweep except the SDT sweep, where the enthalpy differences in the evaporator converged at a SDT = 120 °F (48.89 °C).

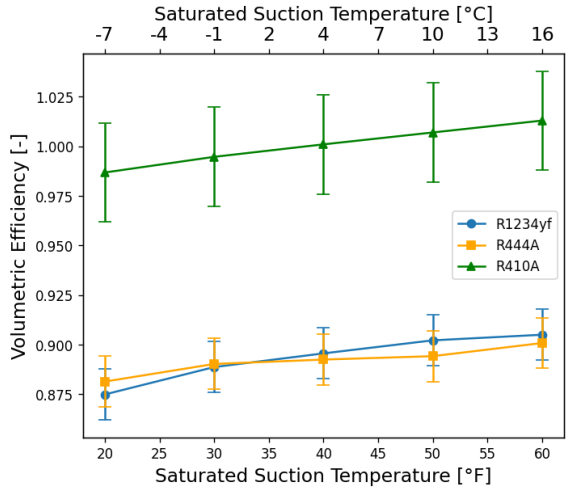

Figure 7: Volumetric efficiency vs SST.

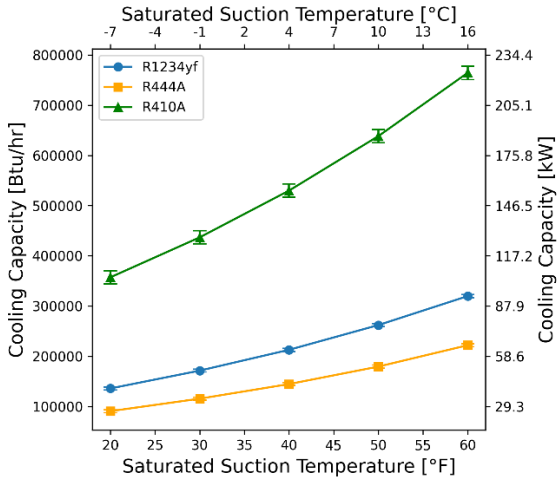

Figure 8: Cooling capacity vs SST.

Finally, as would be expected based on the power consumption and cooling capacity, R-410A has the best COP, followed by R-1234yf, while R-444A by far performed the worst. Overall system performance was at its best at higher SSTs and lower SDTs as Figure 9 and Figure 10 show, though those conditions are where the worst isentropic efficiency for all three refrigerants occurred. At its peak isentropic efficiency at SDT = 110 °F (43.33 °C), R-410A had a COP of 4.22. R-1234yf had its peak isentropic efficiency at the same point as R-410A and had a COP of 3.8 for nearly a 10% decrease from R-410A. R-444A performed much worse than both other refrigerants in the overall system performance, with a COP of 2.4 at its peak isentropic efficiency at a SDT = 120 °F (48.49 °C). There was no point in the entire test matrix where R-1234yf or R-444A outperformed R-410A in the COP, and while R-444A had better isentropic efficiencies overall, the small benefit in compressor performance would not be worth the major loss in overall system performance when R-444A is used over R-1234yf.

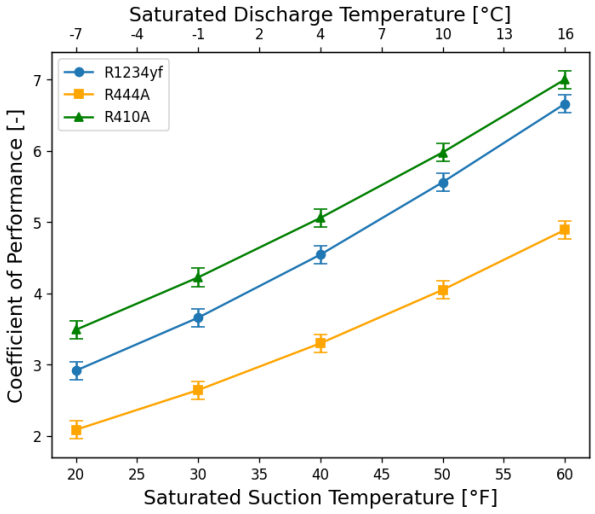

Figure 9: COP vs SST.

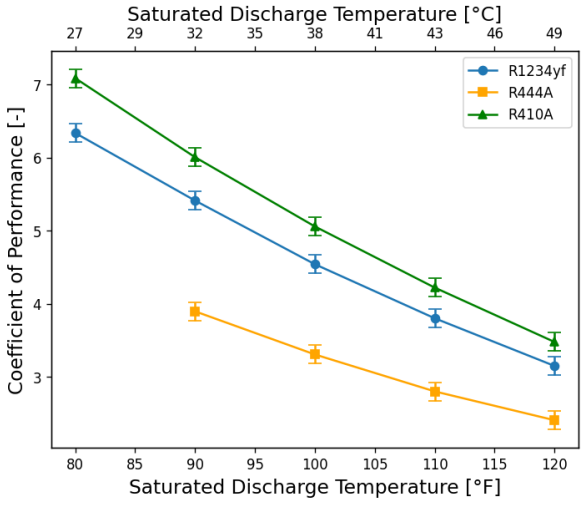

Figure 10: COP vs SDT.

4. CONCLUSIONS

With the current worldwide initiative to replace high GWP refrigerants with low GWP alternatives, there is a challenge to meet current efficiency standards given the loss in thermodynamic efficiency many low GWP refrigerants face. Therefore, it relies on equipment such as the scroll compressor to overcome the loss in refrigerant efficiency. The leakage of scroll compressors is dependent on the operating pressures, which change with the refrigerant used. This paper provides an analysis of several low GWP refrigerants on a commercial scroll compressor designed for R-410A

to quantify the performance losses when these low GWP refrigerants are used. Testing was done on a large hot-gas bypass load stand using R-1234yf and R-444A, while R-410A was simulated using the manufacturer's software. A saturated suction temperature sweep, saturated discharge temperature sweep, speed sweep, and a superheat sweep were performed for a total of 22 datapoints to cover the range of operating conditions on the compressor. Thermodynamically, R-410A has a lower critical temperature and higher operating pressures than both R-1234yf and R-444A, though it has an extremely high GWP of 1890. R-1234yf and R-444A both have low GWPs and similar operating pressures, but different critical temperatures. Test result show that:

- R-410A had 44% and 59% higher mass flow rates from R-1234yf and R-444A respectively, while consuming 55% more power than R-1234yf and 58% more power than R-444A.
- R-410A had isentropic and volumetric efficiencies greater than 10 percentage points than the low GWP refrigerants, with isentropic efficiency peaking at 74.7%.
- R-1234yf had a 26% greater mass flow rate and 6% greater power consumption than R-444A but had 1-3 percentage points smaller isentropic efficiencies. The peak isentropic efficiency of R-1234yf was 64.5% while R-444A had a peak isentropic efficiency of 66.6%
- R-444A had a 44% decrease in cooling capacity from R-1234yf.
- R-410A had the best overall system performance with a COP at peak isentropic efficiency of 4.22. R-1234yf had a COP of 3.8, while R-444A had the lowest COP of 2.4.

R-410A performed better than both R-1234yf and R-444A in every performance metric, with the low GWP refrigerants having a major loss in efficiency and overall system performance. While R-444A had a significantly lower mass flow rate than R-1234yf, it had slightly better isentropic efficiencies due to a higher isentropic enthalpy difference. However, due to the significant loss in cooling capacity and overall system performance R-444A experiences when compared to R-1234yf, it is not worth the small benefit in compressor performance.

NOMENCLATURE

COP	Coefficient of Performance	(-)
η	Efficiency	(-)
GWP	Global Warming Potential	(-)
HFC	Hydrofluorocarbons	(-)
$\dot{m}$	Mass Flow Rate	(lbm/min)
SDT	Saturated Discharge Temperature	(-)
SST	Saturated Suction Temperature	(–)
T	Temperature	(°F)
$\dot{W}$	Power	(kW)
ω	Compressor Speed	(Hz)
$\dot{Q}_{cool}$	Cooling Capacity	(Btu/h)
P	Pressure	(psi)
h	Enthalpy	(Btu/lbm)
V_{disp}	Displacement Volume	(ft^3)
ρ	Density	(lbm/ft^3)

Subscript

1	State1
2	State 2
3	State 3
4	State 4
Cond	Condensing
is	Isentropic
vol	Volumetric
subcool	Subcooling
s	Isentropic

REFERENCES

American Society of Mechanical Engineering (ASME). (2018). PTC-19.1-2013 Test Uncertainty. New York, NY

Creux, L. (1905). *Rotary Engine* (United States Patent Office Patent no 801,182).

Cho, N. K., Youn, Y., Lee, B. C., & Min, M. K. (2000). The Characteristics of Tangential Leakage in Scroll Compressors for Air-Conditioners. *International Compressor Engineering Conference*. International Compressor Engineering Conference.

Domanski, P. A., Steven Brown, J., Heo, J., Wojtusiak, J., & McLinden, M. O. (2014). A thermodynamic analysis of refrigerants: Performance limits of the vapor compression cycle. *International Journal of Refrigeration*, *38*, 71–79. https://doi.org/10.1016/j.ijrefrig.2013.09.036

Elson, J., Kaemmer, N., Wang, S., & Perevozchikov, M. (2008). Scroll Technology: An Overview of Past, Present and Future Developments. *International Compressor Engineering Conference*. International Compressor Engineering Conference, Purdue University.

Lee, B. C., Yanagisawa, T., Fukuta, M., & Choi, S. (2002). A Study on The Leakage Characteristics Of Tip Seal Mechanism In The Scroll Compressor. *International Compressor Engineering Conference*. International Compressor Engineering Conference, Purdue University.

McLinden, M. O., Domanski, P. A., Kazakov, A., Heo, J., & Brown, J. S. (2012). *Possibilities, Limits, and Tradeoffs for Refrigerants in the Vapor Compression Cycle*. National Institute of Standards and Technology.

McLinden, M. O., Kazakov, A. F., Steven Brown, J., & Domanski, P. A. (2014). A thermodynamic analysis of refrigerants: Possibilities and tradeoffs for Low-GWP refrigerants. *International Journal of Refrigeration*, *38*, 80–92. https://doi.org/10.1016/j.ijrefrig.2013.09.032

Mitsuhiro Fukuta, Takeru Sotani, & Masaaki Motozawa. (2021). Leakage and friction characteristics at sliding surface of tip seal in scroll compressors. *International Journal of Refrigeration*, *125*, 104–112. https://doi.org/10.1016/j.ijrefrig.2021.01.016

Tanveer, Mohsin M., & Bradshaw, C. R. (2021). Performance evaluation of low-GWP refrigerants in 1–100 ton scroll compressors. *International Journal of Refrigeration*, *129*, 317–331. https://doi.org/10.1016/j.ijrefrig.2021.05.008

Prapainop, R., & Suen, K. O. (2012). Effects of refrigerant properties on refrigerant performance comparison: A review. *International Journal of Engineering Research and Applications (IJERA)*, *2*(4), 466–493.

Schmidt, D., Singleton, J., & Bradshaw, C. R. (2019). Development of a light-commercial compressor load stand to measure compressor performance using low-GWP refrigerants. *International Journal of Refrigeration*, *100*, 443–453. https://doi.org/10.1016/j.ijrefrig.2019.02.009

Sun, S., Wang, X., Guo, P., Wu, K., Luo, X., & Liu, G. (2019). Numerical analysis of the transient leakage flow in axial clearance of a scroll refrigeration compressor. *Proceedings of the Institution of Mechanical Engineers. Part E, Journal of Process Mechanical Engineering*, *236*(1), 47–61. https://doi.org/10.1177/0954408919870910

Youn, Y., Cho, N. K., Lee, B. C., & Min, M. K. (2000). The Characteristics of Tip Leakage in Scroll Compressors for Air Conditioners. *International Compressor Engineering Conference*. International Compressor Engineering Conference.